Plasmonics (2018) 13:779–784
DOI 10.1007/s11468-017-0572-7

Analysis of a Surface Plasmon Resonance Probe Based on Photonic Crystal Fibers for Low Refractive Index Detection

Chao Liu[1] · Lin Yang[1] · Qiang Liu[1] · Famei Wang[2] · Zhijie Sun[2] · Tao Sun[3] · Haiwei Mu[1] · Paul K. Chu[4]

Received: 31 December 2016 / Accepted: 21 March 2017 / Published online: 29 March 2017

Abstract A photonic crystal fiber (PCF)-based surface plasmon resonance (SPR) probe with gold nanowires as the plasmonic material is proposed in this work. The coupling characteristics and sensing properties of the probe are numerically investigated by the finite element method. The probe is designed to detect low refractive indices between 1.27 and 1.36. The maximum spectral sensitivity and amplitude sensitivity are 6×10^3 nm/RIU and 600 RIU^{-1}, respectively, corresponding to a resolution of 2.8×10^{-5} RIU for the overall refractive index range. Our analysis shows that the PCF-SPR probe can be used for lower refractive index detection.

Keywords Photonic crystal fiber · Surface plasmon resonance · Probe · Finite element method

Introduction

Surface plasmon resonance (SPR) is a unique optical phenomenon arising from optical excitation of charge-density oscillations localized at the interface between a metallic layer and dielectric surface under p-polarized light radiation [1]. As a direct sensing technology, SPR has received much attention because of the excellent sensitivity to changes in refractive indices of the surrounding dielectrics and have potential applications in many fields such as environmental monitoring [2], food safety [3], and biological substance detection [4].

The milestone prototype for SPR sensing proposed by Kretschmann in 1968 was based on the total internal reflection effect of the prism configuration [5]. The p-polarization or transverse magnetic (TM) light impinges a prism coated with plasmonic materials (Au, Ag, Cu, Al, etc.), and the evanescent wave excites the surface plasmon polaritons (SPP) wave [6]. In 1983, Liedberg et al. reported an SPR sensor for biosensing and gas detection [7] and since then, SPR sensing technology has experienced sustainable development in terms of miniaturization and integration based on total internal reflection effect. Since the fiber-based SPR sensors were firstly explored in the early 1990s, many optical fiber SPR sensors with diverse structures such as D-shape, cladding, and TFBG-based have been proposed and investigated experimentally and theoretically [8–12]. Compared with the prism Kretschmann configuration, the fiber-based SPR sensors not only are miniaturized without bulky mechanical components but possess a compact structure suitable for remote sensing. Therefore, the fiber-based SPR sensors can overcome the drawback of bulky conventional SPR configurations.

In recent years, much effort has been devoted to the design of photonic crystal fiber-based SPR (PCF-SPR) [13–16]. The sensing mechanism of PCF-SPR is based on coupling of a leaky core mode to the plasmonic mode along a metalized fiber microstructure. The sensing performance of PCF-SPR sensors depends on the metallic materials. Among the various types of plasmonic materials, gold and silver are the most common ones due to their relatively low loss in the visible

✉ Chao Liu
msm-liu@126.com

✉ Tao Sun
taosun@hotmail.com.hk

[1] School of Electronics Science, Northeast Petroleum University, Daqing 163318, People's Republic of China

[2] School of Materials Science and Chemical Engineering, Harbin Engineering University, Harbin 150001, People's Republic of China

[3] Institute of Microelectronics, Agency of Science, Technology and Research (A*STAR), Singapore 117685, Singapore

[4] Department of Physics and Materials Science, City University of Hong Kong, Tat Chee Avenue, Kowloon, Hong Kong, China

and near-infrared region. This low loss enables the monitoring of high energy transfer on the surface of plasmonic materials during SPR. Many PCF-SPR sensors with diverse structures have been proposed and numerically analyzed. One of the aims of PCF-SPR design is to broaden the detection range of refractive indices for wide applications. R. Otupiri et al. presented a biosensor with a thin gold layer on the inner surface of the microfluidic slots, and a spectral sensitivity lower than 2000 nm/RIU could be obtained for the refractive index range of 1.33–1.34 [17]. Shuai et al. described a multi-core holey fiber-based plasmonic sensor which possessed an average sensitivity of 2929 nm/RIU for the refractive index range between 1.33 and 1.42 [18]. Zhang et al. developed a multi-core photonic crystal fiber SPR sensor with a sensitivity of 3300 nm/RIU, and the refractive index range was 1.41–1.42 [19]. Luan et al. proposed a microstructured optical fiber-based SPR sensor with silver nanolayer as the sensitive material, and a sensitivity of 1600 nm/RIU was achieved for the detection refractive index range of 1.46–1.62 [20]. Based on these typical examples, one can see that previous work on PCF-SPR sensors has mainly concentrated on the refractive index range larger than 1.33 [21–25]. To our best knowledge, little effort has been devoted to PCF-SPR sensors for lower refractive index detection. Low refractive index detection (1.27–1.33) based on PCF-SPR sensing technology exhibits a great potential for mesoporous silica [26], Si nanopillars [27], and electrophoretic medium [28] in the application field of solar cell and display devices. In addition, one of the great challenges for PCF-SPR sensors is to manufacture metalized microstructure in such a small core of PCF. From the perspective of device fabrication, it is a good alternative to synthesize gold nanowires on the surface of fiber core for the sensor.

Herein, a novel PCF-SPR probe with a gold nanowire placed on the outer wall of the fiber core is presented. A large annular analyte channel is designed around the fiber core, and it is intrinsically the detection zone of the probe. The key performance of the probe is investigated by the finite element method (FEM) based on the COMSOL Multiphysics software. The detection range of refractive indices is set to be 1.27–1.36, and a maximum spectral sensitivity of 6×10^3 nm/RIU is achieved. The sensor with the proposed structure is relatively easy to produce because the gold nanowires are on the outer surface of the fiber core.

Simulation Model

The cross-section of the proposed probe is divided into three parts as shown in Fig. 1. The inner part is silica and arranged with 16 air holes, and the analyte channel coated with a gold nanowire is designed as the second part. Pure silica is set as the background materials of the probe, and the Sellmeier equation is applied to calculate the chromatic dispersion [23].

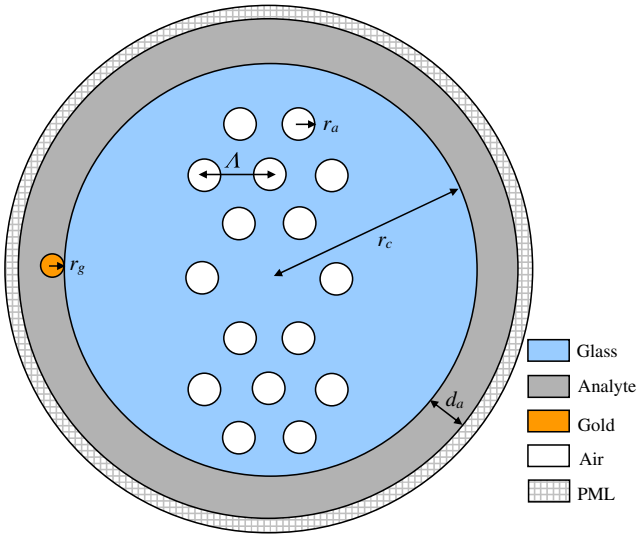

Fig. 1 Schematic diagram of the PCF-SPR probe

Λ = 1.5 μm, d_a = 1.5 μm, r_c = 5 μm, and r_a = 0.32–0.4 μm represent the distance between adjacent air holes, width of the analyte channel, radius of the silica core, and air holes, respectively. The radius of the gold nanowires (r_g) is 0.13–0.2 μm. The air holes with a diameter of 0.8 μm are introduced into the fiber core to reduce the effective refractive index of the core-guided mode to ensure efficient coupling between the core-guided and plasma modes. The refractive indices of the analyte (n_s) vary from 1.27 to 1.36, and the dielectric constant of gold is defined by the Drude mode [15]. The finite element method (FEM) based on the COMSOL Multiphysics software is used to investigate the mode characteristics. An artificial boundary condition of the perfectly matched layer (PML) is added to the outer computational region to absorb the radiation energy. The computational region is meshed with free triangles consisting of 2530 elements and the number of boundary elements is 1299. It is noted that the coupled mode theory is applied to the study of coupling between the plasmonic and core-guided modes [16]. The confinement loss is defined as follows:

$$\alpha_{\text{loss}} = 8.686 \times \frac{2\pi}{\lambda} \text{Im}\left(n_{eff}\right) \times 10^4 (dB/cm), \quad (1)$$

where λ represents the wavelength of the incident light in vacuum with a unit of micrometer (μm). It is proportional to the imaginary part of the effective refractive index. The peak indicates the largest energy transmission from the core-guided mode to the plasmonic mode, and it can be used to locate the resonance wavelength.

The hexagonal air holes confine most of the energy, and a part of the energy penetrates the channel filled with the analyte to excite the plasmon mode of the gold nanowires. There is a strong dependence of the real part of the mode loss on the effective refractive index of the sample, thus making the

wavelength of phase matching between the core-guided and plasmon modes sensitive to the changes in the analyte refractive indices.

Results and Discussion

Figure 2a shows the dependence of real parts and imaginary parts of the effective refractive indices of the fundamental mode on wavelengths. The black and blue curves represent the imaginary and real parts, respectively. The imaginary part of the effective refractive index of the probe is closely related to the mode loss, whereas the real part shows the refractive index in the usual sense. As shown in Fig. 2a, the imaginary part of the refractive index increases initially and then decreases with increasing wavelength. In terms of energy aggregation of the fiber core, an obvious peak occurs at 870 nm when the refractive index of the analyte is 1.35, indicating strong coupling between the plasmonic mode and core guided mode. The electric field intensity distribution of the fundamental mode is presented in Fig. 2b.

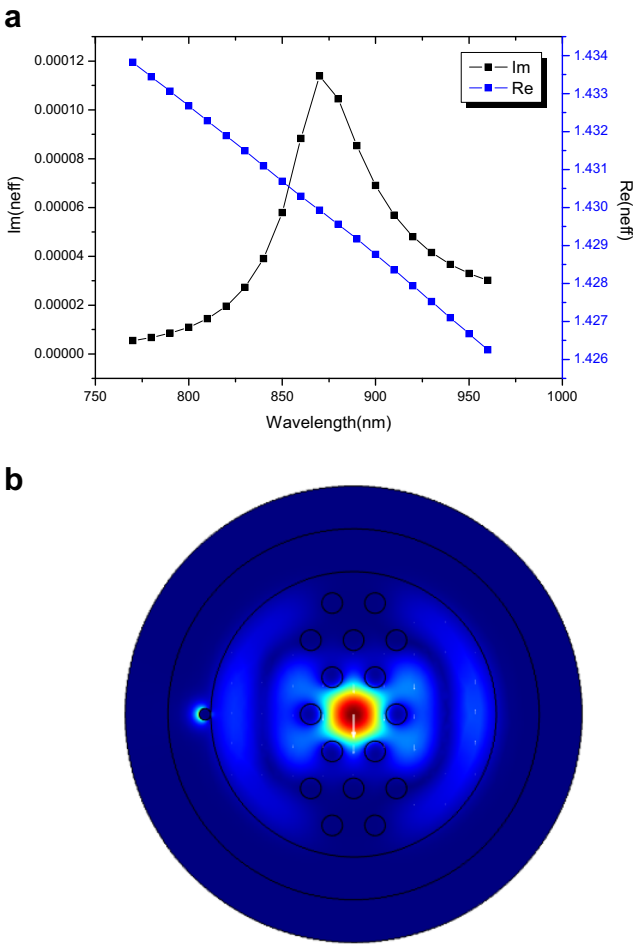

Fig. 2 **a** Dependence of real parts and imaginary parts of the effective refractive indices of the fundamental mode on wavelengths. **b** Electric field intensity distribution of the fundamental mode, where the *arrows* represent the direction of the electric field

The radius of the gold nanowires is one of important parameters affecting the strength and position of the resonance peaks, and so, gold nanowires with different radii are considered here. Figure 3 presents the optical loss spectra of the probe for different radii of gold nanowires. The refractive index of the surrounding medium is set to be n_s = 1.35. Obviously, the resonance wavelength in the near-infrared region moves to longer wavelengths as the gold nanowire radius increases from 0.13 to 0.2 μm. The resonance wavelength shift is approximately 25 nm. There is large energy loss on the surface of gold wires when the radius is between 0.13 and 0.2 μm, indicating that there is an optimal radius for each wavelength. In addition, the resonance intensity decreases gradually with increasing gold nanowire radius and the maximum drop in the intensity is approximately 60 dB/cm. This phenomenon can be explained as follows. The skin depth of gold is about 20–30 nm. When the radiuses of gold nanowires increase, the fiber core mode becomes effectively screened from the plasmon, resulting in a low coupling efficiency and low sensitivity [15].

The fiber core with air holes works as a low refractive index cladding ensuring transmission of mode guidance. The sixteen air holes arranged in the hexagonal array in the probe reduce the refractive index of the core and so the phase matching condition between the core mode and plasmon can be met. Figure 4 shows the dependence of the confinement loss on the size of air holes for different wavelengths. The strength depth increases with the size of the air holes. Larger air holes promote expulsion of the modal field from the fiber core leading to larger modal presence close to the interface of gold and subsequently higher propagation loss. Furthermore, the wavelength red shifts as the air holes become bigger. An obvious absorption peak occurs at 870 nm, and the resonance strength

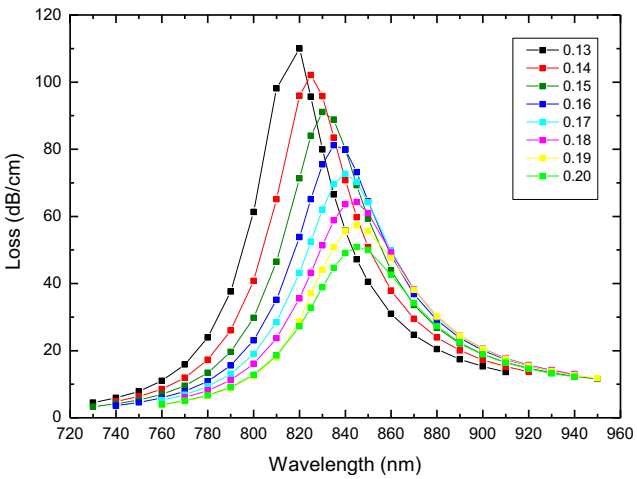

Fig. 3 Optical loss spectra for different radii of gold nanowires (Λ = 1.5 μm, d_a = 1.5 μm, r_c = 5 μm, r_a = 0.36 μm, and n_s = 1.35)

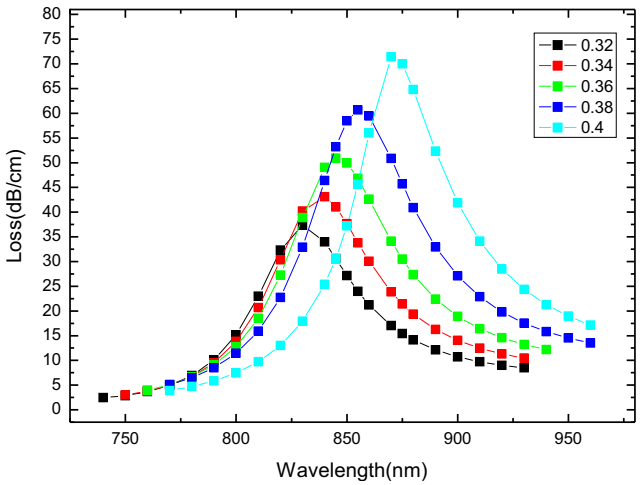

Fig. 4 Dependence of the loss spectra on the radius of the air holes (Λ = 1.5 μm, d_a = 1.5 μm, r_c = 5 μm, n_s = 1.35, and r_g = 0.2 μm)

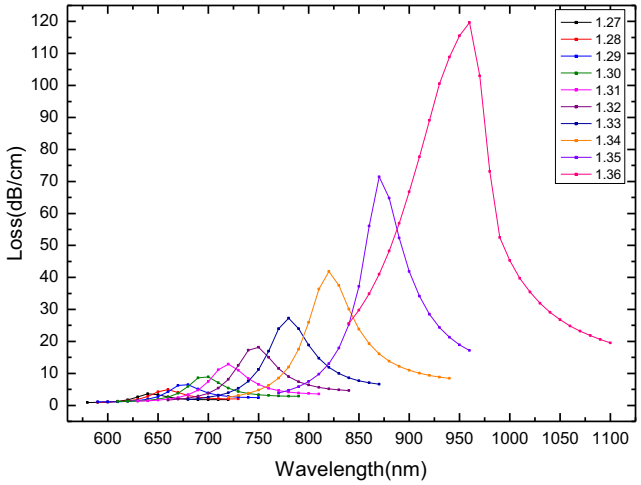

Fig. 6 Loss spectra of the fundamental mode for different analytes (Λ = 1.5 μm, d_a = 1.5 μm, r_a = 0.36 μm, r_c = 5 μm, and r_g = 0.2 μm)

can reach about 73 dB/cm when the radius of the air hole is 0.4 μm.

To determine the effects of the silica core radius on the properties of the proposed probe, the calculated loss spectra are plotted in Fig. 5. The resonance wavelength moves towards longer wavelength, and the resonance strength increases remarkably as the radius of silica core increases from 4.8 to 5.1 μm. When the radius of the silica core is 5.1 μm, there is more leakage of the fundamental mode into the gold nanowire at 850 nm. It can be concluded that plasmonic excitation on gold nanowires is stronger for certain core radii.

Figure 6 shows the optical loss spectra of the probe for different analytes. The resonance wavelength increases from 640 to 960 nm while the refractive index of the analyte changes from 1.27 to 1.36. The corresponding wavelength shift is approximately 320 nm, indicating that the resonance wavelength can be tuned to the near-infrared region. Moreover, the resonance strength shows a positive relationship with the refractive index from 1.27 to 1.36. When the refractive index is 1.36, the resonance strength can be up to 120 dB/cm.

In order to determine the properties of the PCF-SPR probe, the amplitude sensitivity is considered and can be expressed as [15]

$$S_{\mathrm{am}} = \frac{1}{\alpha(\lambda, n)} \frac{\partial \alpha(\lambda, n)}{\partial n} \left(RIU^{-1}\right). \tag{2}$$

The transmission loss $\alpha(\lambda,n)$ refers to the confinement loss α_{loss}. Figure 7 shows that the amplitude sensitivity varies with the wavelength at a refractive index of 1.35. The amplitude sensitivity increases first and then decreases with increasing wavelength and S_{am} can reach about 600 RIU^{-1} at a wavelength of 960 nm. The spectral sensitivity of the probe is

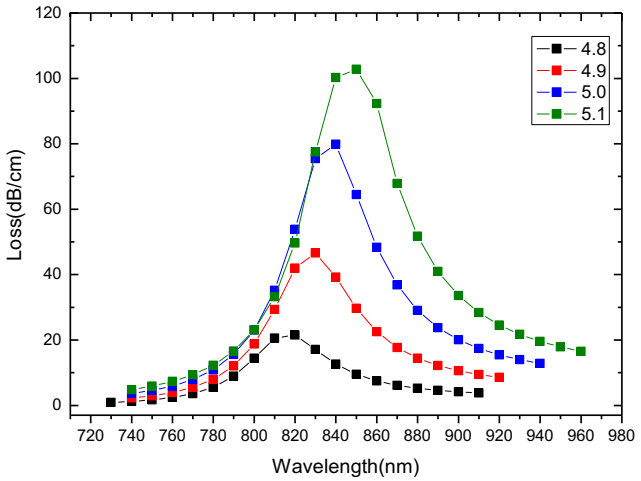

Fig. 5 Loss spectra of the probes with different silica core radii (Λ = 1.5 μm, d_a = 1.5 μm, r_a = 0.36 μm, n_s = 1.35, and r_g = 0.2 μm)

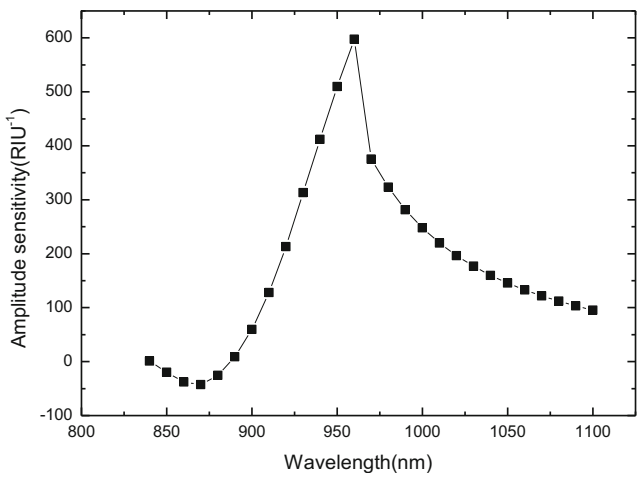

Fig. 7 Amplitude sensitivity of the probe (Λ = 1.5 μm, d_a = 1.5 μm, r_a = 0.36 μm, r_c = 5 μm, and r_g = 0.2 μm)

calculated by detecting the shift in the resonance peaks for different refractive indices of the analytes. The formula for $S_{sp}(\lambda)$ is as follows [29]:

$$S_{sp}(\lambda) = \frac{\Delta\lambda_{\text{peak}}}{\Delta n_{\text{a}}}(nm/RIU), \tag{3}$$

where $\Delta\lambda_{peak}$ and Δn_a represent the resonance wavelength changes and analyte refractive index variation, respectively. When the refractive index of the sample is in the range of 1.27–1.33, each change of 0.01 in the refractive index will shift the loss spectrum curve by 23.5 nm on the average, indicating that the spectral sensitivity of 2350 nm/RIU can be attained. Similarly, the spectral sensitivity is approximately 6×10^3 nm/RIU when the refractive index of the sample varies between 1.33 and 1.36. The refractive index resolution (R) of the probe is calculated by the following eq. [30]:

$$R = \Delta n_a \Delta\lambda_{\text{min}}/\Delta\lambda_{\text{peak}}. \tag{4}$$

Here, $\Delta\lambda_{peak} = 36$ nm is the average wavelength shifts for the refractive index ranges from 1.27 to 1.36. The wavelength resolution is assumed to be $\Delta\lambda_{\text{min}} = 0.1$ nm [16, 17, 19, 21]. When the variation in the analyte index is 0.01, a sensing resolution of 2.8×10^{-5} RIU is accomplished for the refractive index range between 1.27 and 1.36.

Conclusion

A PCF-SPR probe with gold nanowires as the plasmonic material is proposed for low refractive index detection. The probe possesses one large size microfluidic channel which can avoid channel interference with each other. This structure is easy to produce as there is only one gold nanowire close to the silica core. The probe has high sensitivity in the low refractive index range between 1.27 and 1.36, and the spectral sensitivity is approximately 2350 nm/RIU for the refractive index range between 1.27 and 1.33. The spectral sensitivity is 6×10^3 nm/RIU for analyte refractive indices from 1.33 to 1.36. A sensing resolution of 2.8×10^{-5} RIU is realized for the overall refractive index range detection. Our analysis shows that the PCF-SPR probe has large potential in low refractive index detection.

Acknowledgements This work was supported by the National Natural Science Foundation of China (Grant No. 51474069), China Postdoctoral Science Foundation funded project (Grant No. 2016 M59150), Natural Science Foundation of Heilongjiang Province (Grant No. E2016007), and City University of Hong Kong Applied Research Grant (ARG) No. 9667122 and Strategic Research Grant (SRG) No. 7004644.

References

1. Alexandre GB (2012) Plasmonics for future biosensors. Nat Photonics 6:709–613
2. Kim YC, Cramer J, Battaglia T, Jordan JA, Soame NB, Peng W, Laurel LK, Karl SB (2013) Investigation of in situ surface plasmon resonance spectroscopy for environmental monitoring in and around deep-sea hydrothermal vents. Anal Lett 46(10):1607–1617
3. Chen ST, Mark HM, Christopher TE, Jos B (2010) Advances in surface plasmon resonance biosensor technology towards high-throughput, food-safety analysis. TrAC Trends Anal Chem 29(11):1305–1315
4. Li L, Zhang X, Liang Y, Guang J, Peng W (2016) Dual-channel fiber surface plasmon resonance biological sensor based on a hybrid interrogation of intensity and wavelength modulation. J Biomed Opt. doi:10.1117/1.JBO.21.12.127001
5. Kretschmann E, Raether H (1968) Radiative decay of non-radiative surface plasmons excited by light. Zeitschrift Für Naturforschung A 23(12):2135–2136
6. Gupta B, Verma R (2009) Surface plasmon resonance-based fiber optic sensors: principle, probe designs, and some applications. Journal of Sensors 2009:1–12
7. Liedberg B, Nylander C, Lunström I (1983) Surface plasmon resonance for gas detection and biosensing. Sensors Actuators 4(2): 299–304
8. Gasior K, Martynkien T, Wojcik G, Mergo P, Urbanczyk W (2016) D-shape polymer optical fibres for surface plasmon resonance sensing. Opto-Electronics Review 24(4):209–215
9. Cao J, Tu MH, Sun T, Grattan KTV (2013) Wavelength-based localized surface plasmon resonance optical fiber biosensor. Sensors Actuators B Chemical 181(5):611–619
10. Shevchenko Y, Francis T, Derosa M, Albert J (2011) Surface Plasmon resonance optical fiber biosensor for label-free characterization of biomolecular interactions. Bio-optics: Design and Application 36(9):1121–1136
11. Marquez-Cruz V, Albert J (2015) High resolution NIR TFBG-assisted biochemical sensors. J Lightwave Technol 33(16):3363–3373
12. Shevchenko Y, Chen C, Dakka MA, Albert J (2010) Polarization-selective grating excitation of plasmons in cylindrical optical fibers. Opt Lett 35(5):637–639
13. Jitendra ND, Rajan J (2014) Graphene based birefringent photonic crystal fiber sensor using surface plasmon resonance. IEEE Photon Technology Letters 26:1092–1095
14. Hassani A, Skorobogatiy M (2006) Design of the microstructured optical fiber-based surface plasmon resonance sensors with enhanced microfluidics. Opt Express 14(24):11616–11621
15. Hassani A, Skorobogatiy M (2009) Photonic crystal fiber-based plasmonic sensors for the detection of bio-layer thickness. Journal of the Optical Society of America B-Optical Physics 26(8):1550–1557
16. Hautakorpi M, Mattinen M, Ludvigsen H (2008) Surface-plasmon-resonance sensor based on three-hole microstructured optical fiber. Opt Express 16(12):8427–8432
17. Otupiri R, Akowuah EK, Haxha S (2014) A novel Birefrigent photonic crystal fiber surface plasmon resonance biosensor. IEEE Photonics Journal 6(4):1–11
18. Shuai BB, Li X, Zhang YT, Liu DM (2012) A multi-core holey fiber based plasmonic sensor with large detection range and high linearity. Opt Express 20:5974–5986
19. Zhang PP, Yao JQ, Cui HX, Lu Y (2013) A surface plasmon resonance sensor based on a multi- core photonic crystal fiber. Optoelectron Lett 9(5):342–345
20. Luan NN, Yao JQ, Wang R, Hao CJ, Wu BQ, Duan LC, Lu Y (2013) Numerical investigation of the microstructured optical fiber-based surface plasmon resonance sensor with silver nanolayer. Appl Mech Mater 411:1573–1576

21. Yu X, Zhang Y, Pan SS, Shum P, Yan M, Leviatan Y, Li CM (2009) A selectively coated photonic crystal fiber based surface plasmon resonance sensor. J Opt 12:74–77
22. Rifat AA, Mahdiraji GA, Shee YG, Shawon MJ, Adikan FRM (2016) A novel photonic crystal fiber biosensor using surface plasmon resonance. Procedia Engineering 140:1–7
23. Patnaik A, Senthilnathan K, Jha R (2015) Graphene-based conducting metal oxide coated d-shaped optical fiber spr sensor. IEEE Photon Technol Lett 27(23):1–1
24. Zheng L, Zhang X, Ren X, Gao J, Shi L, Liu X, Wang Q, Huang Y (2011) Surface plasmon resonance sensors based on ag-metalized nanolayer in microstructured optical fibers. Opt Laser Technol 43(5):960–964
25. Shuai BB, Xia L, Liu DM (2012) Coexistence of positive and negative refractive index sensitivity in the liquid-core photonic crystal fiber based plasmonic sensor. Opt Express 20(23):25858–25866
26. Shieh JM, Wu SC, Ni WX, Kuo HC, Lai YF, Hsiang KC, Chen YC (2007) Enhanced light transmission for Si solar cells using antireflector of mesoporous silica with low refractive index. Lasers and Electro-Optics Society. doi:10.1109/LEOS.2007.4382410
27. Lin GR, Chang YC, Liu ES, Kuo HC, Lin HS (2007) Low refractive index Si nanopillars on Si substrate. Appl Phys Lett 90:1819231–1819233
28. Whitehea LA (2001) Enhanced effective refractive index total internal reflection image display, United States Patent 6304365
29. Zhou C (2013) Theoretical analysis of double-microfluidic-channels photonic crystal fiber sensor based on silver nanowires. Opt Commun 288:42–46
30. Hautakorpi M, Mattinen M, Ludvigsen H (2014) Surface-plasmon-resonance sensor based on three-hole microstructured optical fiber. Opt Express 16(12):8427–8432